Mesoscopic dynamics of inhomogeneous polymers based on variable cell shape dynamic self-consistent field theory

Xuan Li, Ping Tang,[a),b)] Hongdong Zhang, Feng Qiu, and Yuliang Yang[a),c)]
Key Laboratory of Molecular Engineering of Polymer, Ministry of Education, and Department of Macromolecular Science, Fudan University, Shanghai 200433, People's Republic of China

(Received 7 December 2007; accepted 9 January 2008; published online 17 March 2008)

In this paper, we combine variable cell shape method with dynamic self-consistent field theory and extend to study structure and dynamics under shear for triblock copolymer melts. Due to shear, the calculation cell shape is variable and no longer orthogonal. Pseudospectral method is employed to solve the diffusion equation for chain propagator on the nonorthogonal coordinate and the shear periodical condition can be easily designed in terms of the variable cell shape method. By using this strategy, the shear induced morphology evolution is investigated for topologically complex polymeric systems such as linear and star triblock copolymers; the morphology of linear *ABC* triblock copolymers is more shear sensitive than that of star triblocks. In particular, once the chain propagator is obtained, the microscopic elastic stress and spatial stress distribution can be derived and thus the dynamic mechanical property can be calculated under shear. By imitating the dynamic storage modulus G' corresponding to any given morphology in the oscillatory shear measurements, we explore the relationship between the morphology and the storage modulus G' and extend to study the mechanism of phase separation dynamics as well as order-disorder transition (ODT) for linear and star triblock copolymers. The results show that the chain architecture can be easily distinguished by investigating the ODT, though the systems such as *AB* symmetric diblock and *ABA* triblock copolymers by coupling *AB* precursors almost exhibit similar microstructures. In addition, the storage modulus G' and loss modulus G'' can be simultaneously determined in frequency sweeps of oscillatory shear measurements and the dependence of the moduli on phase separated patterns and the chain topology is investigated. The simulation findings are in qualitatively agreement with the experimental results. © *2008 American Institute of Physics*.
[DOI: 10.1063/1.2839306]

I. INTRODUCTION

Due to microphase separation, block copolymers can self-assemble into a variety of ordered structures such as lamellae (LAM), hexagonally packed cylinders, and body centered cubic spheres and more complex structures such as gyroid (G) in melts and solutions.[1] The self-consistent field theory (SCFT) has been successful in predicting the equilibrium self-assembled morphologies of complex multiblock copolymers in bulk[2–4] due to the development of real-space implementation of SCFT by Drolet and Fredrickson.[5] Recently, such a method has been extended to investigate the aggregation behavior of *AB* diblock copolymers and *ABC* triblock copolymers in solution.[6] In contrast to equilibrium microphase morphologies of block copolymers,[7,8] however, the behavior of block copolymer melts in out of equilibrium such as under shear is not fully understood. In fact, the rheology and shear oriented morphology of phase separated complex polymer fluids are of great importance due to the wide area of industrial applications and its technological importance in polymer processing. In particular, block copolymers with different architectures result in different morphologies and hence significant differences in thermodynamics and rheological behavior.[9]

Although continuous media mechanics and powerful molecular models especially the reptation model and its various extensions have proven to be successful in theoretical study of dynamics and rheology for homogeneous polymer melts and solutions,[10] they have not had similar success for inhomogeneous system such as phase separated polymer blends, block copolymers, etc. In this regard, phenomenological mesoscopic dynamic models known as the time dependent Ginzburg–Landau (TDGL) theory and two-fluid model have received much attention to deal with the viscoelastic behavior and dynamics along with the time evolution of morphologies and rheology in complex liquids under external flows.[11] Unfortunately, these models involve a large number of phenomenological parameters, such as the description of stress, and are inevitably not easy to capture the detail of the chain topology and difficult to introduce the inhomogeneity to the flow field; hence, they are limited for applications for complex multiblock copolymers. In contrast, recently, much work has been done to address this problem by combining the field theory with the dynamic method. Ganesan and Pryamitsyn combined SCFT with Brownian dynamics to study the dynamics and rheology of inhomoge-

[a)]Authors to whom correspondence should be addressed.
[b)]Electronic mail: pingtang@fudan.edu.cn.
[c)]Electronic mail: yuliangyang@fudan.edu.cn.

neous polymer blends[12] and polymer blend interfaces.[13] A dynamic variant of mean-field theory known as the dynamic density functional theory proposed by Fraaije, combining the generalized TDGL, has been demonstrated to be a powerful method to describe the mesoscopic dynamics of inhomogeneous polymeric system.[14] Accordingly, the advances of this method have allowed one to investigate the morphology and dynamical characteristics of block copolymers with different architectures under flow,[15] but the stress and strain variables were not included in their model. On the other hand, SCFT for dense polymer melts has been proven to be highly successful in describing complex morphologies and mechanical properties such as tensile modulus in block copolymers.[16] In particular, The introduction of strain field in the SCFT proposed by Fredrickson[17,18] allows investigating the mechanical properties for inhomogeneous block copolymers. Recently, the hydrodynamic effect was further incorporated in the field theory to investigate the phase separation kinetics of triblock copolymers in a submicron chanel.[19] In contrast to the phenomenological calculation of stress,[20] SCFT considers the chain conformation and thus discerns topological characteristics of the chain. Additionally, the recent variable cell shape method in field theory simulations, which is proposed by Fredrickson, allows the cell shape changes in order to automatically relax the morphologies to a stress-free equilibrium state.[18] We suppose that this method could be used for dealing with the phase behavior of in homogeneous polymer system under shear.

The morphologies as well as dynamics of block copolymers are strongly affected by topological constraints. In this regard, our primary objective in this article is to present a theoretical model based on the combination of the variable cell shape SCFT method[18] with dynamic SCFT (DSCFT) scheme adopted by our group[21] to investigate the morphologies and dynamic issues for phase separated multiblock polymers such as linear and star triblock copolymers subjected to shear. This modified DSCFT method not only can be used to describe the dynamics of block copolymer melts under external shear but also can be used to obtain the microscopic elastic stress according to the deformation and to study the relationship between morphology and the rheological properties. To our knowledge, this is the first simulation to observe the morphology kinetics and the resulting mechanical properties for block copolymers with a specific topological structure. The simulation cell subjected to shear and cell deformation is strain controlled: therefore, the calculation cell can be described according to the idea of variable cell shape scheme and, moreover, internal stress and its distribution can be expressed in terms of the single-chain propagator $q(\mathbf{r},s)$ computed in the field-theoretic simulation.

II. THEORETICAL METHOD

SCFT is known to be an appropriate and accurate theory to be used for simulating equilibrium morphologies of block copolymers with different chain architectures such as linear and star *ABC* triblock copolymers.[2,3] DSCFT is the nonequilibrium version of SCFT used for dealing with the dynamics. In this section, we will mainly show how the variable cell shape SCFT algorithm is combined with the modified DSCFT to deal with the dynamics of *ABC* triblock copolymers with different architectures under shear.

We consider linear *ABC* triblock copolymers of volume V, containing n Gaussian chains. Each copolymer chain consists of N segments with the block ratio f_A, f_B, and $f_C=1-f_A-f_B$ for blocks A, B, and C, respectively. In order to simulate nonequilibrium microphase separation kinetics under external fields for complex architecture block copolymers, the TDGL is combined with the SCFT, known as the DSCFT, to describe the dynamics of inhomogeneous system. In DSCFT, to embed the dynamic process, the phase separation kinetics under shear is assumed to obey the modified TDGL equation for conserved order parameter,[22]

$$\frac{\partial \phi_I(\mathbf{x},t)}{\partial t} = M_I \nabla^2 \frac{\delta F[\phi_I(\mathbf{x})]}{\delta \phi_I} - \mathbf{v}(\mathbf{x}) \cdot \nabla \phi_I(\mathbf{x},t) + \eta_I, \qquad (1)$$

where $\phi_I(\mathbf{x},t)$ $(I=A,B,C)$ represents the monomer density fields of species I at position $\mathbf{x}$ and time t, M_I is the segment mobility coefficient of species I, which is assumed to be a constant, and $\mathbf{v}(\mathbf{x})$ stands for the flow field. In our two-dimensional (2D) simulations, the deformation is strain controlled, the velocity direction is along the x axis, and the velocity gradient direction is along the y axis, i.e., $v_x=\dot{\gamma}y$ and $v_y=0$ for simple steady shear and $v_x=\Gamma y\omega \cos \omega t$ and $v_y=0$ for externally imposed oscillatory shear flow. $\dot{\gamma}$ is the reduced shear rate (time derivative of the strain γ), Γ is the amplitude of the oscillatory shear strain, and ω is the angular frequency. η_I stands for the Gaussian thermal noise with the zero mean and satisfies the fluctuation-dissipation relation. $\mu_I(\mathbf{x})=\delta F[\phi_I(\mathbf{x})]/\delta\phi_I(\mathbf{x})$ represents the intrinsic nonequilibrium chemical potentials, where $F[\phi_I(\mathbf{x})]$ is the free energy functional, which is not easy to be accurately and systematically obtained by traditional phenomenological cell dynamics simulations (phase-field model) especially for complex block copolymers with a specific chain architecture. Therefore, in DSCFT, the following trick is used to obtain the chemical potentials of block copolymers.[21] The hypothetical external potentials $U_I(\mathbf{x})$ that act on the I species are introduced to counterbalance the current chemical potentials $\mu_I(\mathbf{x})$, i.e., $U_I(\mathbf{x})=-\mu_I(\mathbf{x})+\xi(\mathbf{x})$, which drives and updates the current density profile $\phi_I(\mathbf{x},t)$ to an equilibrium state. The Lagrange multiplier $\xi(\mathbf{x})$ is chosen to be $\xi(\mathbf{x})=\lambda[1-\phi_A(\mathbf{x})-\phi_B(\mathbf{x})-\phi_C(\mathbf{x})]$ to ensure the incompressibility of the system,

$$\begin{aligned} U_A(\mathbf{x}) &= w_A(\mathbf{x}) - \chi_{AB}\phi_B(\mathbf{x}) - \chi_{AC}\phi_C(\mathbf{x}), \\ U_B(\mathbf{x}) &= w_B(\mathbf{x}) - \chi_{AB}\phi_A(\mathbf{x}) - \chi_{BC}\phi_C(\mathbf{x}), \\ U_C(\mathbf{x}) &= w_C(\mathbf{x}) - \chi_{AC}\phi_A(\mathbf{x}) - \chi_{BC}\phi_B(\mathbf{x}), \end{aligned} \qquad (2)$$

where χ_{IJ} is the dimensionless Flory–Huggins interaction in units of k_BT and $w_I(\mathbf{x})$ is the self-consistent field exerted to species I, which is determined by adjusting it iteratively with the steepest descent method using Eq. (1) to coincide with the density profiles $\phi_I(\mathbf{x},t)$ calculated by the SCFT equations.

In SCFT, the statistics of a copolymer chain are subjected to a set of effective chemical potential fields w_I which

replace the actual interactions between different components and are conjugated to the segment density fields ϕ_I of block species I. The density profiles $\phi_I(\mathbf{x},t)$ are obtained through the calculation of the characteristic single-chain propagator $q(\mathbf{x},s)$ in the deformable cell due to shear. We follow the variable cell shape method proposed by Barrat *et al.*[18] to describe the polymer morphological behavior in deformable calculation cell due to shear deformation. The variable shape cell is described by a 2×2 shape matrix $\mathbf{h}$ in 2D,

$$\mathbf{h} = \begin{vmatrix} h_{xx} & h_{yx} \\ h_{xy} & h_{yy} \end{vmatrix} = \begin{vmatrix} L_x & L_y \cos\alpha \\ 0 & L_y \sin\alpha \end{vmatrix}$$

for a 2D $L_x\times L_y$ cell, where L_x and L_y are side length of the cell and α is the angle between adjacent sides, to hold all the points $\mathbf{R}$ in Cartesian coordinates expressed as $\mathbf{R}=\mathbf{hx}$, where $\mathbf{x}$ is a rescaled vector whose components lie in $[0, 1]$. Integrals on $\mathbf{R}$ can be converted into integrals over $\mathbf{x}$ by using a scaling factor $\det\mathbf{h}$ ($\det\mathbf{h}=V$) representing the volume of the calculation cell. A metric tensor constructed by $\mathbf{G}=\mathbf{h}^T\mathbf{h}$ is used to transform dot products from original Cartesian to rescaled coordinates. Thus, for linear ABC triblock copolymers, $q(\mathbf{x},s)$ is given by a modified diffusion equation

$$\frac{\partial q(\mathbf{x},s)}{\partial s} = \frac{b^2}{6}\frac{(\mathbf{G}^{-1})_{\alpha\beta}\partial^2 q(\mathbf{x},s)}{\partial x_\alpha \partial x_\beta} - [\gamma_A(s)w_A(\mathbf{x},s) + \gamma_B(s)w_B(\mathbf{x},s) + \gamma_C(s)w_C(\mathbf{x},s)]q(\mathbf{x},s), \quad (3)$$

with the initial condition $q(\mathbf{x},0)=1$. b is the statistical segment length of chains of three species, α and β stand for two orthogonal coordinates in original Cartesian and we take the Einstein implicit summation notation for the repeated alternate Greek indices, and $\gamma_I(s)$ is 1 if s belongs to block I and otherwise 0. Because the two ends of triblock chains are distinct, a second end-segment distribution function $q^+(\mathbf{x},s)$ is further needed that can be similarly obtained with the right side of Eq. (3) multiplied by -1, subjected to the initial condition $q^+(\mathbf{x},N)=1$. The density of triblock copolymers is thus obtained by

$$\phi_A(\mathbf{x}) = \frac{V}{NQ}\int_0^{Nf_A} ds q(\mathbf{x},s)q^+(\mathbf{x},s),$$

$$\phi_B(\mathbf{x}) = \frac{V}{NQ}\int_{Nf_A}^{N(f_A+f_B)} ds q(\mathbf{x},s)q^+(\mathbf{x},s), \quad (4)$$

$$\phi_C(\mathbf{x}) = \frac{V}{NQ}\int_{N(f_A+f_B)}^{N} ds q(\mathbf{x},s)q^+(\mathbf{x},s),$$

where $Q=\int d\mathbf{x} q_K(\mathbf{x},s)q_K^+(\mathbf{x},s)$ is the partition function of a single chain. The extension to star ABC triblock copolymers is straightforward.

In contrast to traditional TDGL, the above modified DSCFT implicitly updates the chemical potential fields w_I by SCFT, which is capable of simulating the microphase separation kinetics for various architecture block copolymers. In addition, we note that hydrodynamic effects are not included in this DSCFT scheme, which are important especially in the low molecular weight system. Very recently, the hydrodynamic effect was first incorporated in the field theory called HSCFT by Hall *et al.* to simulate more realistic complex fluid flows.[19] However, in this paper, as a first step, we focus on the simple shear induced aligned morphologies; the macroscopic linear shear rate is chosen to overwhelm the hydrodynamic effect. Moreover, in the study of order-disorder transitions, we aim at detecting the elastic response of ordered domains, and thus the segment diffusion terms are switched off and hydrodynamic effects can be neglected. We expect the hydrodynamics to have little effects on the study of systems subjected to simple shear, and our simulation tests confirmed this expectation.

Once the chain propagator is obtained, the elastic stress for linear ABC triblock copolymer can be written[18] as

$$\frac{\sigma_{\alpha\beta}}{(n/V)k_BT} = \frac{b^2}{6Q}h_{\gamma\alpha}^{-1}h_{\delta\beta}^{-1}\int d\mathbf{x}\left(\int_0^N ds q(\mathbf{x},s)\frac{\partial^2 q^+(\mathbf{x},s)}{\partial x_\alpha \partial x_\beta} + \int_0^N ds q^+(\mathbf{x},s)\frac{\partial^2 q(\mathbf{x},s)}{\partial x_\alpha \partial x_\beta}\right). \quad (5)$$

The free energy functional (in units of nK_BT/V) is thus given by

$$F = (1/V)\int d\mathbf{x}[\chi_{AB}\phi_A\phi_B + \chi_{BC}\phi_B\phi_C + \chi_{AC}\phi_A\phi_C - \omega_A\phi_A(\mathbf{x}) - \omega_B\phi_B(\mathbf{x}) - \omega_C\phi_C(\mathbf{x}) - \xi(1-\phi_A-\phi_B-\phi_C)] - \frac{1}{N}\ln Q/V + \beta V(\boldsymbol{\sigma}:\boldsymbol{\varepsilon}), \quad (6)$$

where the last term in Eq. (6) is the contribution of stress $\boldsymbol{\sigma}$ and strain $\boldsymbol{\varepsilon}$ to the free energy for an incompressible triblock copolymer melt in a cell of variable shape, in which the strain is given by $\boldsymbol{\varepsilon}=\frac{1}{2}[(\mathbf{h}_0^T)^{-1}\mathbf{G}(\mathbf{h}_0)^{-1}-1]$ and $\mathbf{h}_0$ is the original cell shape of the simulation box before deformation.

According to the calculated stress in Eq. (5), the storage modulus G' and loss modulus G'' in traditional oscillatory shear tests can be derived by linear fitting the simulated stress-strain curve as follows:

$$\sigma_{\alpha\beta}^{\text{int}} = \Gamma[G'\sin(\omega t) + G''\cos(\omega t)]. \quad (7)$$

In this simulation, we first only focus on the case that the microphase separation process of block copolymers is decoupled with rheological measurements, and thus $G''=0$. The storage modulus, therefore, can be obtained by analyzing the stress-strain relation, i.e., $G'=\sigma_{\alpha\beta}^{\text{int}}/[\sin(\omega t)\Gamma]$. Secondly, in the frequency sweeps measurements, the diffusion ($M\neq0$) is switched on and G' as well as G'' can be derived by linear fitting the simulated stress-strain curve of Eq. (7).[20,23]

In Eqs. (1), (3), and (5), the Laplacian operator $(\mathbf{G}^{-1})_{\alpha\beta}\partial^2/\partial x_\alpha\partial x_\beta$ is required to be solved in nonorthogonal coordinates when the simulation cell is deformed to parallelogram from rectangle. The Laplacian in orthogonal coordinates can be discretized by the Crank–Nicholson or the alternating direction implicit (ADI) scheme in the real-space implementation of SCFT. It is evident that this method is not available in nonorthogonal coordinates. In this simulation, a pseudospectral algorithm, first brought forward to solve the single-chain propagator equation of SCFT by Tzeremes

et al.,[24] is borrowed to numerically solve the Laplacian in nonorthogonal coordinates by using twice Fourier transforms.[18]

Unlike the previous treatment of sheared periodical conditions, i.e., Lee–Edwards boundary condition in molecular dynamics simulations,[25] it becomes convenient to solve numerical breakdown problems due to the introduction of the shape matrix for the variable shape cell. In the case of simple steady shear, $\dot{\gamma}$ is the reduced shear rate scaled by the box size h_{yy} (L_y), and the accordingly reduced strain γ is the deformation scaled by the box size. When shear is imposed, in the time region $(0<t<1/\dot{\gamma})$, namely, within one integral times the deformation of the box size, Eqs. (1), (3), and (5) with Laplacian operator are solved in deformed cells, and the beveled horizontal component of cell shape matrix becomes $h'_{xy}=h_{xx}\times\dot{\gamma}t$ accordingly. Then, we stop shear when the strain is increased to the box size, $t=1/\dot{\gamma}$, $\gamma=h_{xy}/h_{xx}=1$, i.e., the beveled horizontal element of cell shape matrix becomes $h'_{xy}=h_{xx}\times 1$, while the other matrix components are kept unchanged. The data $\omega'_I(\mathbf{r}',1/\dot{\gamma})$ and $\phi'_I(\mathbf{r}',1/\dot{\gamma})$ on the rescaled coordinate (x',y') are transformed to $(x'-L_x,y)$ for $L_x\leqslant x'\leqslant 2L_x$ and thus $\mathbf{h}'$ is back to the orthogonal coordinate again. Then, restart the shear by using the updated data ω_I and ϕ_I as the next initial values and continue to deform the new cell. When the strain is again increased to the box size, the above described coordinate transformation will be done. The periodical boundary condition under shear is thus implemented by such iteration steps.

III. RESULTS AND DISCUSSION

The following simulations investigate the influence of the chain architecture such as *ABC* linear and star triblock copolymers on the microphase separation morphologies and dynamic properties under shear by our modified DSCFT with the variable cell shape method mentioned in the previous section. Compared to diblock copolymers, the additional block in triblock copolymers implies additional variables, expands the phase complexity, and results in largely unpredictable morphologies. Therefore, for the sake of simplicity, we assume symmetric interactions between different blocks, i.e., $\chi_{AB}=\chi_{BC}=\chi_{AC}=\chi$, and thus the effect of the copolymer composition on the phase behavior is highlighted. The triblock copolymer chain lengths are set to be $N=100$. Reduced shear rate for simple steady shear is $\dot{\gamma}=10^{-3}$. In the large strain amplitude oscillatory shear (LAOS), the strain amplitude is $\Gamma=0.10-0.50$ and the reduced frequency is $\omega=0.02-0.50$. In the case of elastic modulus (G') analysis, the strain amplitude is fixed to be $\Gamma=0.01$ and the reduced frequency $\omega=0.02$ to ensure that the system is in the linear viscoelastic region. Due to the unbearable consumption of time in three-dimensional (3D) calculation, the simulations are carried out in a 2D 36×36 square lattice with the grid size of $\Delta x=\Delta y=1$ nm. We note that the simulation is repeated with a reasonable range of calculation size to ensure that these obtained morphologies are not influenced by the lattice size. The morphology is indicated with different colors, where blue, green, and red colors are assigned to *A*, *B*, and *C* species, respectively. Hereafter, we use $A_xB_yC_z$ with *x*, *y*, and *z* representing the block ratio f_A, f_B, and f_C, respectively.

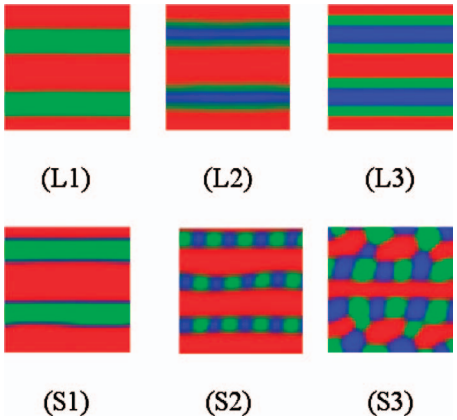

FIG. 1. (Color) The effect of steady shear on the morphology of linear *ABC* triblock (top row) and star *ABC* triblock (bottom row) copolymers under reduced shear rate of $\dot{\gamma}=1.0\times 10^{-3}$. The block ratios from left to right columns are $A_{0.1}B_{0.3}C_{0.6}$, $A_{0.2}B_{0.2}C_{0.6}$, and $A_{0.3}B_{0.3}C_{0.4}$.

A. Effect of shear on the morphology

Figure 1 shows the oriented structure of *ABC* linear triblock copolymers compared to *ABC* star triblock copolymers under simple steady shear $\dot{\gamma}=1.0\times 10^{-3}$ with symmetric interaction parameter $\chi=0.35$. In the left column of Fig. 1 (L1 and S1) for $A_{0.1}B_{0.3}C_{0.6}$, when the lengths of two minority blocks *A* and *B* are evidently unequal, both linear and star triblock copolymers prefer the *A*-*B*-*C* three-layer lamellae (LAM_3) structure, while the core-shell hexagonal lattice (CSH) and LAM_3 are the equilibrium morphology in quiescent condition for linear and star triblock copolymers, respectively. Therefore, linear triblock copolymers are more sensitive to the shear imposed than star terpolymers, as a result of characteristic topological differences: in linear triblock copolymers, the minority *A* block is dispersed in the middle of lamellae formed by block *B* to avoid extra contact enthalpy with majority block *C* lamellae, while in star triblock copolymers, the *A* block is forced to locate at the *B*/*C* interface due to the core chains that prefer lower extensions of the core blocks and form the lamellae phase. In columns (2) and (3) of Fig. 1, where the two immiscible minority blocks (blocks *A* and *B* of $A_{0.2}B_{0.2}C_{0.6}$ and $A_{0.3}B_{0.3}C_{0.4}$) are equal, the *A*-*B*-*C* three-layer LAM structure is still preferred in linear *ABC* triblock, while star triblock copolymers form multicompartmental lamellar structure with two minority blocks *A* and *B* forming alternative lamellae in majority block domains, as a result of the equivalent competences along the shear direction of the two minority blocks in the junction point. Especially for the equal composition of $A_{0.3}B_{0.3}C_{0.4}$, of which the equilibrium morphology in quiescent condition is the stable honeycomb phase, it still keeps a similar honeycomb shape under moderate shear $\dot{\gamma}=1.0\times 10^{-3}$ and forms a multicompartmental lamellae structure after further increasing the shear velocity to $\dot{\gamma}=2.0\times 10^{-3}$ (not shown). Therefore, the previous results suggest that shear stabilizes the lamellae like structure and the morphol-

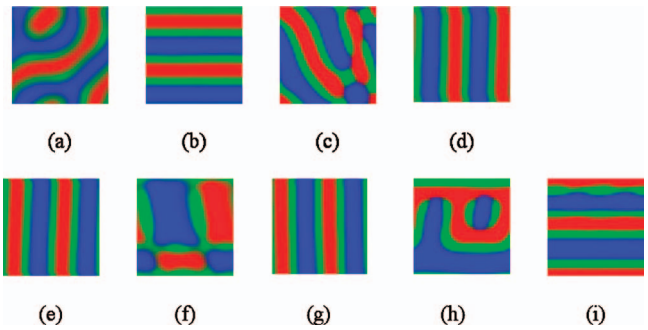

FIG. 2. (Color) The effect of simulated reciprocating oscillatory shear on the orientation of lamellae formed by linear *ABC* triblock copolymer $A_{0.4}B_{0.3}C_{0.3}$. (a) $\Gamma=0.10$ and $\omega=0.02$; (b) $\Gamma=0.25$ and $\omega=0.02$; (c) $\Gamma=0.10$ and $\omega=0.10$; (d) $\Gamma=0.25$ and $\omega=0.10$; (e) $\Gamma=0.10$ and $\omega=0.25$; (f) $\Gamma=0.50$ and $\omega=0.25$; (g) $\Gamma=0.10$ and $\omega=0.50$; (h) $\Gamma=0.25$ and $\omega=0.50$; (i) $\Gamma=0.60$ and $\omega=0.60$.

ogy of linear triblock copolymers is more sensitive to the external shear imposed than that of star terpolymers with the same composition. This may be explained by the topological differences that linearly connected blocks are more flexible to the stretching force and more likely to be extended along the shear direction, while the joint core in star terpolymers is a stronger constraint subjected to shear, resulting in less sensitive changes upon shear.

As discussed above, the shear has strong effect on the morphology of linear *ABC* triblock copolymers. Vigild *et al.* experimentally reported the effect of large amplitude oscillatory shear on the alignment of a lamellae-forming pentablock copolymer.[26] They reported that the medium or large amplitude preferred the perpendicular and transverse orientations. Figure 2 presents the lamellae orientation subjected to the imposed large strain amplitude reciprocating oscillatory shear (LAOS) for $A_{0.4}B_{0.3}C_{0.3}$ linear triblock copolymers forming lamellae in quiescent condition. In order to obtain the influence of shear on the morphology, the assigned oscillatory shear in Fig. 2 is applied in the start of phase separation and thus the shear and morphology evolution occur simultaneously. When the reduced frequency is relatively low, such as $\omega=0.02$, at small strain amplitude in the linear viscoelastic region, the shear only induces the local orientation leading to a partially ordered lamellae structure, shown in Fig. 2(a). As we increase the strain amplitude to $\Gamma=0.25$, lamellae structure parallel to the shear direction [Fig. 2(b)] occur even with a very large strain amplitude (not shown here) due to the large stretching strain along the shear direction. When the reduced frequency is increased to $\omega=0.10$, the shear induced morphologies vary from slanted and twisted lamellae [Fig. 2(c)] to perpendicular to the shear direction lamellae [Fig. 2(d)]. With further increasing the reduced frequency to $\omega=0.25$ and even to $\omega=0.50$, we observe a lamellae structure perpendicular to the shear direction occurring at the small strain amplitude $\Gamma=0.1$, shown in Figs. 2(e) and 2(g), while the mixed morphology of lamellae perpendicular and parallel to the shear direction is observed, as shown in Figs. 2(f) and 2(h). In the extreme cases of Figure 2(i), at $\Gamma=0.60$ and $\omega=0.60$, parallel lamellae are obtained as a result of intensified horizontal stretching.

From the above observations, we conclude that increasing the shear frequency always prefers perpendicular lamellae, while increasing the shear amplitude would rather prefer the parallel lamellar alignment along the shear direction. Therefore, only parallel to shear direction lamellae can be found at a relatively low shear frequency, while perpendicular lamellae occur at a high shear frequency with a small amplitude. Moreover, mixed morphologies of parallel and perpendicular lamellae take place at high frequency with medium amplitude. When parallel stretching outweighs the perpendicular combinational preference in the large amplitude and high frequency region, parallel lamellae are observed again.

B. Morphology evolution and resulting mechanical properties

Due to the importance of dynamic rheological properties in the polymer processing, the phase separated morphology with the resulting dynamic storage modulus G' is studied in this section. In order to explore the influence of topological differences on phase separation kinetics, the morphology and corresponding rheological properties are presented. During this process, the time evolution of phase separation and rheological analysis are decoupled, i.e., rheological measurement is carried out to just obtain G' corresponding to a given morphology in the quiescent phase separation process at every particular time interval (such as 200–300 numerical steps in our simulation). Furthermore, strain amplitude and reduced frequency are set to be $\Gamma=1\%$ and $\omega=0.02$ to ensure that the oscillatory shear measurement is in linear viscoelastic regime. The diffusion term is switched off, i.e., $M=0$ during rheological measurement to avoid possible effect of shear on the morphology evolution, and also we have confirmed that after the diffusion term is switched off, reduced frequency will not affect G' in a wide linear viscoelastic range, such as $\omega=0.001-0.1$. In addition, the loss modulus is nearly zero under this simplification and only the storage modulus may be determined.[20]

Figure 3 presents the topological effect of *ABC* triblock copolymers on the time evolution of G' and phase separated morphologies at particular phase separation stage. The comparisons are taken among the same compositions of $A_{0.2}B_{0.2}C_{0.6}$ for linear *ABC* triblock copolymers with different chain sequences and star *ABC* triblock polymers $A_{0.2}B_{0.2}C_{0.6}$, with equal interaction energies between each species, i.e., $\chi=0.35$. The terminal equilibrium structures reproduce our previous simulated results using the static SCFT method.[2,3] The total modulus G' and the separate modulus contributions G'_A, G'_B, and G'_C from blocks *A*, *B*, and *C*, respectively, are calculated. In *A* and *C* composition asymmetric linear $A_{0.2}B_{0.2}C_{0.6}$ triblock copolymer of Fig. 3(a), the system is quenched from a disordered state at time $t=0$. After a short time until $t<1500$, as a result of both increases in concentration fluctuations and specific interfacial areas during the coarsening of domains, the moduli G'_A, G'_B, and G'_C increase rapidly, and so does the total modulus G'. Then, with the concentration fluctuations being saturated, initially formed domains are reorganized and separated from each other to form ordered structures. It is interesting to note that from $t=1500$ to $t=2500$, the moduli from blocks *A* and *C*

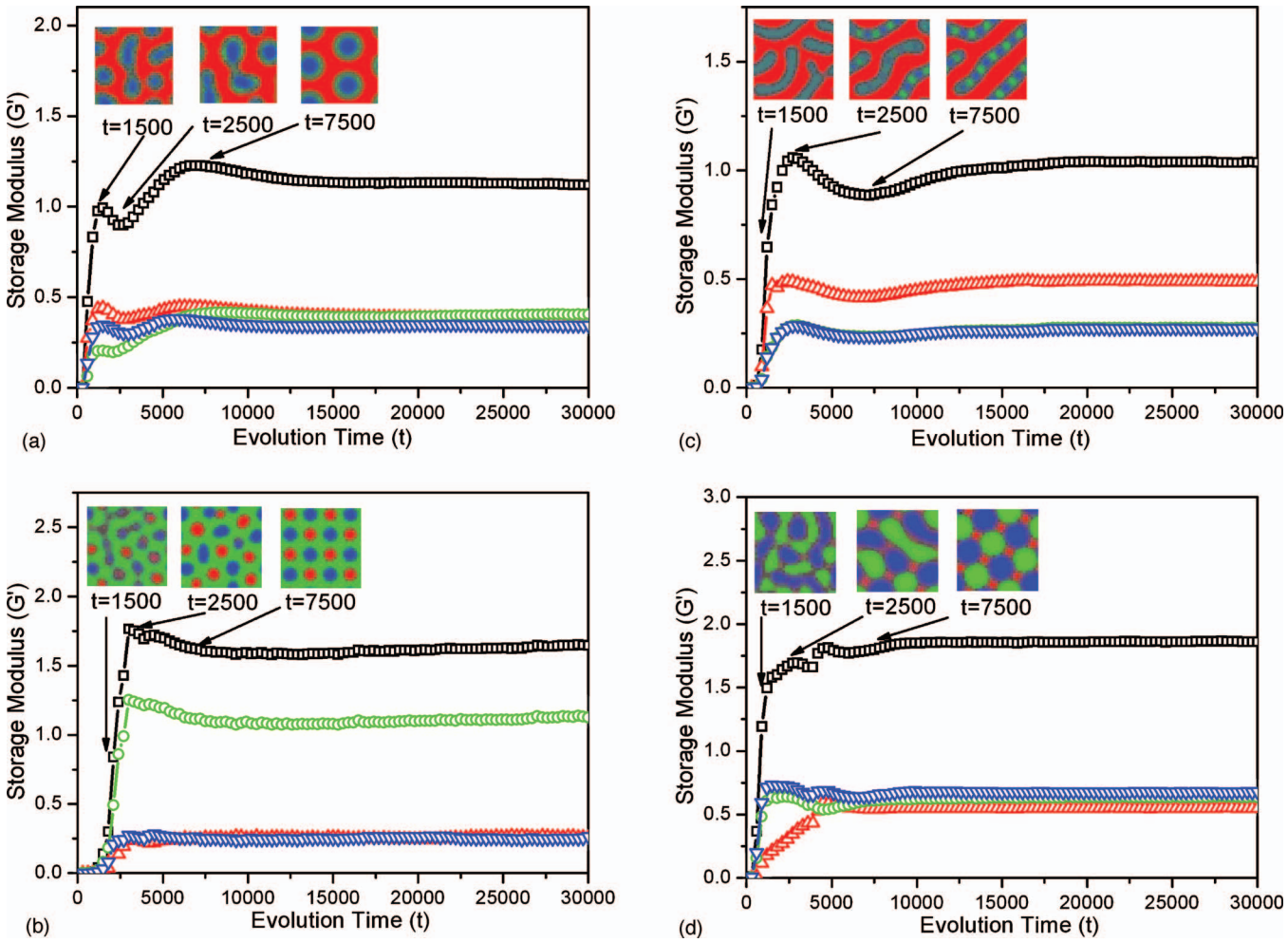

FIG. 3. (Color) Phase separation morphology and corresponding G' (in units of nK_BT/V) with time evolution at $\chi=0.35$. (a) linear $A_{0.2}B_{0.2}C_{0.6}$ (CSH), (b) linear $A_{0.2}B_{0.6}C_{0.2}$ (TET_2), (c) star $A_{0.2}B_{0.2}C_{0.6}$ (LAM+BD), and (d) star $A_{0.4}B_{0.4}C_{0.2}$ (octagon-octagon-tetragon phase). G' (□), G'_A (▽), G'_B (○), and G'_C (△). The inset shows corresponding morphologies at certain stage of phase separation.

simultaneously decrease after the peak value, indicating that interfacial areas of blocks A and C reduce correspondingly; moreover, modulus of blocks B keeps no dramatic changes. We assume that during this period, phase separation of species B is trapped at the interface between blocks A and C due to the topological link of blocks B to A and C, resulting in the modulus of blocks B being "frozen" at this stage of phase separation. The possible phase separation kinetics can be that majority blocks C are first separated from the mixed A and B domains, then blocks A and B are further separated from each other. In the intermediate stage of phase separation (from $t=2500$ to $t=5000$), the CSH structure is found and blocks A and C are separated from each other, with B domains covering A domains to avoid direct contacts from C species. As a result, G'_A and G'_C continue to decrease, while the B block is located between A and C and the amount of A/B and B/C interfaces is not changed, but the interfaces become clearer, leading to a slight increase in the G'_B. At the later stage of phase separation ($t>7500$), a completely ordered CSH structure is formed and thus the modulus is stabilized.

For symmetric composition with respect to blocks A and C of a linear $A_{0.2}B_{0.6}C_{0.2}$, as shown in Fig. 3(b), i.e., by changing the sequence of blocks B and C of Fig. 3(a), three moduli from three species A, B, and C simultaneously increase to the peak value at $t=2500$. In contrast to Fig. 3(a), blocks A, B, and C phase separate synchronically and thus the incubation time is longer than that of the case in Fig. 3(a), resulting in three moduli increasing simultaneously due to the symmetric end block composition. After the peak, the moduli are quickly stabilized and two-interpenetrating-tetragonal lattice phase (TET_2) is formed with A and C interpenetrating cylinders in the majority B matrix.[2] For the star triblock copolymer $A_{0.2}B_{0.2}C_{0.6}$ with the same composition as Figs. 3(a) and 3(b), it is also observed that three species are simultaneously separated from each other and three block moduli increase to peak values at $t=2500$, as shown in Fig. 3(c). After the modulus peak, lamellae phase with B and C alternating beads (LAM+BD) is found and the modulus is thus stabilized. This is similar to the case of Fig. 3(b), but the terminal plateau modulus is smaller than that of linear triblock copolymers as a result of the distinctive decrease of interfacial areas in star $A_{0.2}B_{0.2}C_{0.6}$ compared to linear $A_{0.2}B_{0.6}C_{0.2}$. In Fig. 3(d), the equilibrium octagon-octagon-tetragon phase is observed for star $A_{0.4}B_{0.4}C_{0.2}$, consistent with our previous static SCFT simulations.[3] It should be noted that a similar modulus "trap mode" of the minority

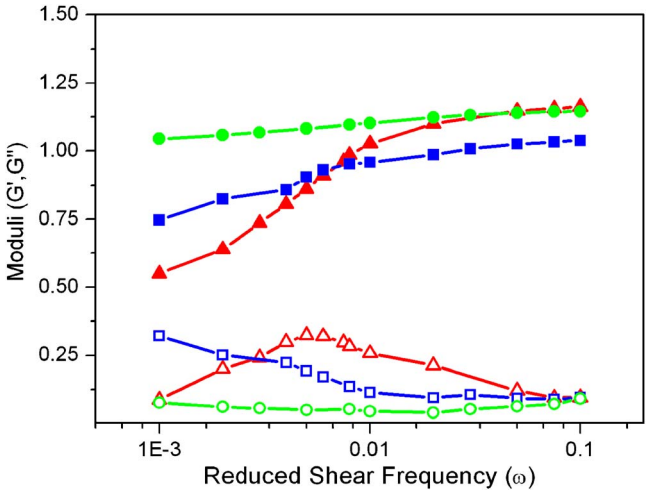

FIG. 4. (Color online) Simulation results of G' and G'' (in units of nK_BT/V) in frequency sweep measurement at strain amplitude $\Gamma=0.01$ for linear and star *ABC* triblock copolymers (evolution time $t=30\,000$ and $\chi=0.35$). Linear $A_{0.2}B_{0.2}C_{0.6}$, G' (■) and G'' (□); linear $A_{0.2}B_{0.6}C_{0.2}$, G' (▲) and G'' (△); star $A_{0.2}B_{0.2}C_{0.6}$, G' (●) and G'' (○).

component *C* (the minority block *C* is gradually separated from blocks *A* and *B*) is also observed in Fig. 3(d) for star $A_{0.4}B_{0.4}C_{0.2}$ to that of linear $A_{0.2}B_{0.2}C_{0.6}$ with the minority middle block *B* in Fig. 3(a). However, this is not found in Figs. 3(b) and 3(c). The phenomena result from different dynamical mechanisms of phase separation, as discussed in Fig. 3(a).

In addition, as mentioned in Sec. II, the storage modulus G' and loss modulus G'' can be simultaneously determined in frequency sweeps when we do not close the diffusion ($M \neq 0$) in the simulation of rheological response. The typical samples are taken from the terminal equilibrium states (evolution time $t=30\,000$) of equilibrium morphologies of Figs. 3(a)–3(c). The plots of G' and G'' versus ω at strain amplitude $\Gamma=0.01$ are shown in Fig. 4. To avoid the effect of shear stress on the morphology evolution at extremely lower frequency (lower shear stress), the frequency sweeps are taken between $\omega=0.001$ and 0.1, and the resulting G', G'' are averaged by two shear directions (*X* and *Y*). Although we did not consider the time-temperature shift factor, Fig. 4 still shows qualitatively the dependence of the moduli on phase separated patterns and chain topology. As the morphologies studied are in the intermediate segregation regime where three blocks are phase separated from each other, the low shear stress induced is mostly of elastic origin and the changes of G' are more obvious than those of G''. It is interesting to note that lamellar structures of star $A_{0.2}B_{0.2}C_{0.6}$ (LAM+BD) and linear $A_{0.4}B_{0.4}C_{0.2}$ (LAM_3, not shown here) all exhibit a typical solid response, i.e., less sensitive of G' and G'' to the frequency sweep and quite small G'' in all frequency regions, because lamellar structures are highly ordered and not able to be deformed much in the presence of low shear stress. However, cylindrical structures of linear $A_{0.2}B_{0.2}C_{0.6}$ (CSH) and linear $A_{0.2}B_{0.6}C_{0.2}$ (TET_2) show a typical solid response in the relatively high frequency region and viscous responses in the relatively lower frequency sweeping impact. In particular, the unexpected increase of G'' of linear $A_{0.2}B_{0.6}C_{0.2}$ (TET_2) in the relatively slow frequency region ($\omega=0.001-0.05$) can be attributed to the flexibility of (TET_2) cylinders to the low shear stress.

Furthermore, it is interesting to note that local stress distribution originated from changes in the chain conformations through the chain propagator according to Eq. (5) may be calculated for *ABC* linear triblock and star triblock copolymers. Figure 5 presents unique equilibrium morphologies of LAM_3, CSH phases in quiescent condition for linear *ABC* triblock copolymers, and LAM+BD phases for *ABC* star triblock copolymers, as well as the corresponding distribution of local stress tensor components. Figures 5(b) and 5(c) show the spatial distribution of stress tensor component σ_{XX} and stress profile of σ_{XX} close to the interfaces because the lamellae perpendicular to the *X* axis only support the stress along the *X* direction. From Fig. 5(c), we also observe a decrease of the stress at the center of interface and a slight increase of stress a few lattices farther from the interface which approaches zero to the interior of a lamellar domain. These results are in accordance with the stress distribution in diblock copolymers by Maniadis *et al.*[27] As explained by Maniadis *et al.*,[27] the chain segments are stretched more than average due to the repulsive interaction between different block species in the interface region; the stress in this region becomes large. Comparing the stress distribution of linear triblock and star triblock copolymers with the same composition in Figs. 5(d)–5(i), the axial stress tensor component σ_{XX} in the CSH phase of linear $A_{0.2}B_{0.2}C_{0.6}$ in Fig. 5(e) exhibits a similar cylindrical stress distribution to that of asymmetric diblock copolymers,[27] with the maximal negative value of stress at the outer B/C interface and maximal positive value of stress in the inner A/B interface. Another interesting phenomenon is that the additional middle block *B* introduces a wide zero stress space interval and serves more like a thick stress-free interface. Stress tensor component σ_{XY} plotted in Fig. 5(f) exhibits a symmetric nonorthogonal stress distribution where the stress is mainly distributed along the diagonal direction of the *XY* plane. In star $A_{0.2}B_{0.2}C_{0.6}$ [LAM+BD phases in Fig. 5(g)], as shown in Fig. 5(h), σ_{XX} presents a characteristic alternating stress distribution; the maximal negative value of stress is located at the minority A/B interfaces where interfacial segments are strongly stretched due to the incompatibility between blocks *A* and *B*, and the maximal positive value of stress is observed in the interior of cylindrical domains where segments of homogeneous blocks *A* (*B*) are compressed. Due to the horizontal orientation of the lamellae and beads, the stress σ_{YY} (not shown here) is mainly distributed in lamella/bead interfaces where star junction points are located. Moreover, the nonorthogonal stress component σ_{XY} of star $A_{0.2}B_{0.2}C_{0.6}$ in Fig. 5(i) tends to distribute alternatively in the interfaces where the junction points are located. From the above observations, we may conclude that the stress with the maximal negative value is located on the interfaces due to the strong repulsion of each other of immiscible blocks in the interfaces.

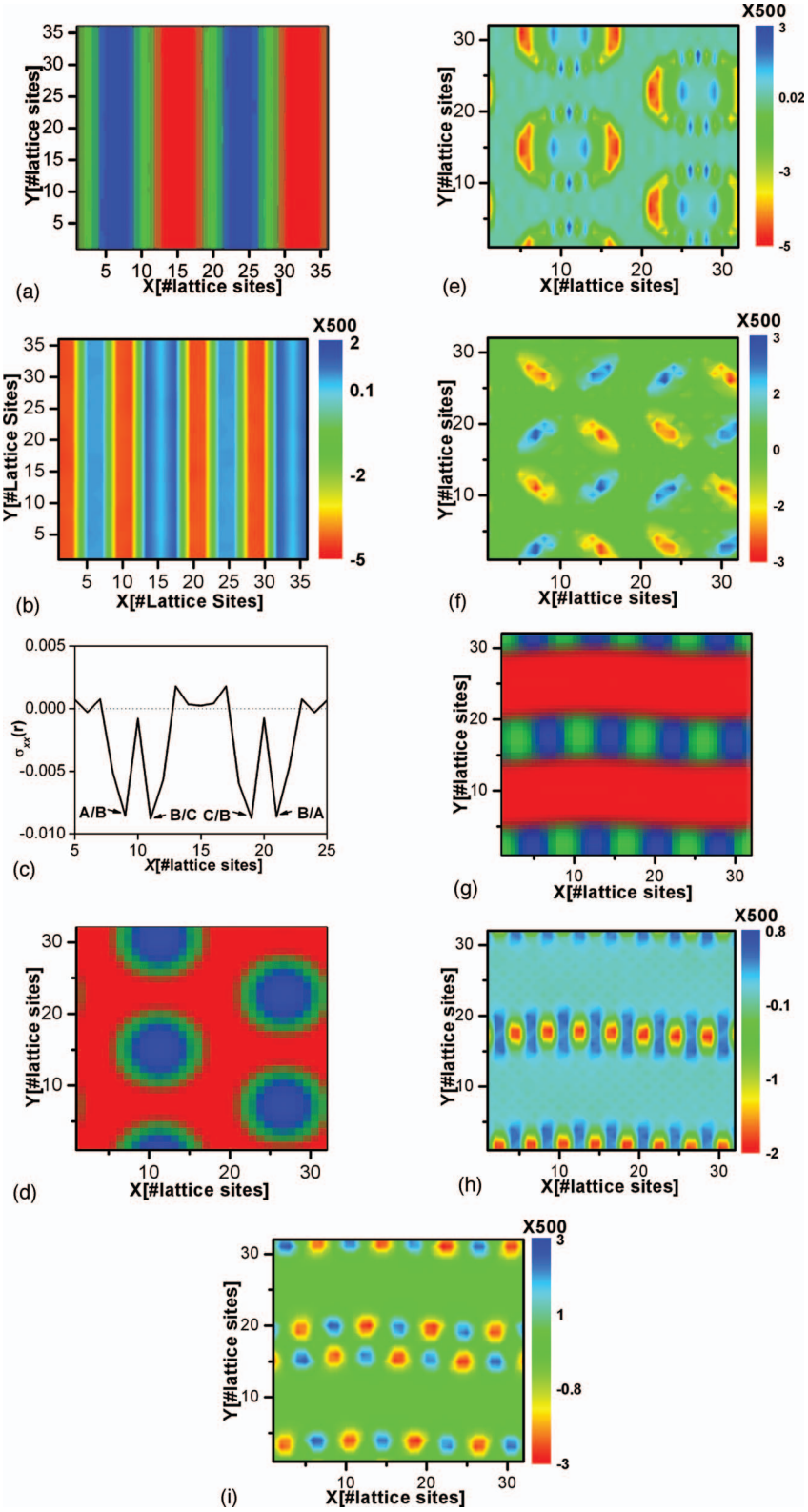

FIG. 5. (Color) Equilibrium phases and corresponding distribution of stress tensor components in *ABC* linear triblock copolymers $A_{0.3}B_{0.3}C_{0.4}$ (top row), $A_{0.2}B_{0.2}C_{0.6}$ (middle row), and star *ABC* terpolymers $A_{0.2}B_{0.2}C_{0.6}$ (bottom row). The morphology density is shown in (a) for LAM_3, (d) for CSH, and (g) for LAM+BD phases. The corresponding stress tensor components σ_{XX} (in units of nK_BT/V) are shown in the middle column and σ_{XY} (in units of nK_BT/V) are shown in the right column, except that (c) presents the stress profile of σ_{XX} (in units of nK_BT/V) close to an interface in (b) for LAM_3.

C. The ODT and OOT determined from dynamic storage modulus

In the past two decades, numerous experimental and theoretical studies for block copolymers have been reported on how the phase transitions, i.e., an order-disorder transition (ODT) and order-order transition, depend on block composition and temperature.[1,8] Rheological measurements are very sensitive to identify the ODT and order-to-order transition (OOT) (the transition from one ordered state to another) in contrast to morphology transitions. However, as we are aware, little theoretical work has been done on the simulation of rheological measurements to derive the ODT in complex topological block copolymers. The present method, variable cell shape DSCFT, is able to correlate the structure with dynamic storage modulus, thus providing us additional means of studying ODT/OOT. In this work, the dependence

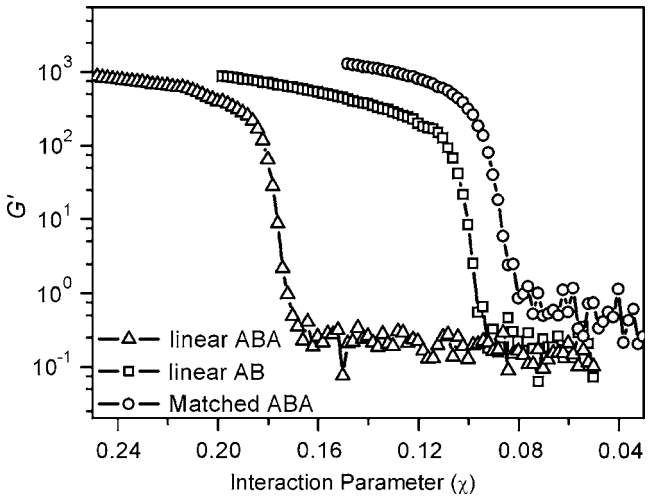

FIG. 6. Simulated temperature sweep of G' (in units of nK_BT/V) for symmetric AB diblock ($f=0.5$), ABA triblock with each A block being of equal length, and ABA triblock copolymers by coupling the symmetric AB diblock precursor. The species are subjected to oscillatory shear flow at strain amplitude $\Gamma=0.01$ and reduced frequency of $\omega=0.02$. Three moduli are vertically shifted by 3 decades for clarity.

of G' at a fixed frequency as a function of χN corresponding to the temperature due to the inverse relationship between the temperature T and Flory–Huggins interaction parameter χ is simulated for ABC linear and star triblock copolymers. We will show how this method can be used to obtain the ODT.

In the study of order-to-disorder and order-to-order transitions of block copolymers, temperature sweep of storage modulus G' and loss modulus G'' during heating with a constant rate was employed to investigate the ordering kinetics of different morphologies in block copolymers. In our simulations, temperature sweep is implemented by continuously slowly decreasing the interaction parameter χ at which the phase separation is evolved to equilibrium, and subsequently rheological measurement is carried out at fixed strain amplitude $\Gamma=0.01$ and reduced frequency $\omega=0.02$. The G' vs χ is thus obtained and the χ at which the slope of curve G' vs χ abruptly changes is labeled as χ_{ODT} and χ_{OOT}; corresponding temperatures are T_{ODT} and T_{OOT}. Additionally, the extremely slow change rate in χ ($\Delta\chi/t=0.001/1000$) is chosen in our simulations to ensure that each tested morphology is in near equilibrium under corresponding segregation conditions. It should be noted that from the experimental point of view, for a highly asymmetric block copolymer, the ordering of the microdomain during cooling from a disordered state to an ordered state is very slow compared with the disordering of the microdomain during the heating process from the ordered state to the disordered state. Thus, in experiments, temperature sweep of G' during heating is more powerful to detect the transition temperature, while in the simulation, cooling and heating processes obtain almost the same temperature sweep curves because the simulation is carried out under the ideal circumstances and only considers the modulus related to the given morphology.

Figure 6 presents the temperature sweep of G' during heating [changes of Flory–Huggins (FH) interaction parameters from $\chi=0.25$ to $\chi=0.02$] for a symmetric AB diblock with $f_A=0.5$, ABA triblock with $f_A=0.5$ and each A block being of equal length, and ABA triblock copolymers by coupling symmetric diblock precursor with $2N$ chain length. Although these copolymers adopt similar microstructures (not shown here), the chain configurations are indeed different which is evident in critical ODT values, as shown in Table I. From Fig. 6 and Table I, the ODT for AB diblock copolymers is $\chi_{\mathrm{ODT}}=0.105$ at $f=0.5$ with $N=100$, which is consistent with the theoretical phase diagrams[8] and prediction of $\chi N=10.5$ for the symmetric diblock copolymer with $f=0.50$ by Leibler based on random phase approximation theory.[28] For the case of $A_{0.25}B_{0.5}A_{0.25}$ triblock with $N=100$ and $A_{0.25}B_{0.5}A_{0.25}$ triblock copolymers obtained by coupling two symmetric AB diblocks, thus leading to $N=200$, the ODTs are calculated to be $\chi_{\mathrm{ODT}}=0.185$ and $\chi_{\mathrm{ODT}}=0.092$, respectively, very close to the literature predictions of $\chi N=18$.[29]

TABLE I. Calculated χ_{ODT} for block copolymers with different compositions. Literature χ_{ODT} values of diblock copolymers are labeled with asterisks in the bracket.

Block copolymers	χ_{ODT}
Diblock $A_{0.5}B_{0.5}(N)$	0.105(0.105*)
Triblock $A_{0.25}B_{0.5}A_{0.25}(N)$	0.185(0.18*)
Triblock $A_{0.25}B_{0.5}A_{0.25}(2N)$ by Coupling AB diblocks	0.092(0.09*)
Linear $A_{0.5}B_{0.1}C_{0.4}(N)$	0.11
Linear $A_{0.5}B_{0.4}C_{0.1}(N)$	0.12
Linear $A_{0.3}B_{0.3}C_{0.4}(N)$	0.15
Linear $A_{0.7}B_{0.1}C_{0.2}(N)$	0.17
Star $A_{0.5}B_{0.1}C_{0.4}(N)$	0.14
Star $A_{0.7}B_{0.1}C_{0.2}(N)$	0.20
Star $A_{0.3}B_{0.4}C_{0.3}(N)$	0.22

Figures 7(a) and 7(b) present the temperature sweep of G' during heating (changes of FH interaction parameters from $\chi=0.70$ to $\chi=0.0$) for linear and star ABC triblock copolymers, respectively. Figure 7(a) gives the χ (temperature) dependence of G' during the dynamic temperature sweep measurement for linear triblock copolymer $A_{0.5}B_{0.1}C_{0.4}$, showing initially a slowly gradual decrease in G' until a significant drop of G' at $\chi=0.11$. The precipitous decrease in G' is therefore regarded as the $\chi_{\mathrm{ODT}}=0.11$. This result is almost the same with that of AB diblock copolymers due to the low composition of middle block B in linear triblock $A_{0.5}B_{0.1}C_{0.4}$.

Table I shows the χ_{ODT} from the calculation of AB diblock, ABA linear triblock, ABC linear triblock, and star triblock copolymers with similar compositions. For linear triblock copolymers, we clearly find that $\chi_{\mathrm{ODT}}(A_{0.5}B_{0.1}C_{0.4}) < \chi_{\mathrm{ODT}}(A_{0.3}B_{0.3}C_{0.4}) < \chi_{\mathrm{ODT}}(A_{0.7}B_{0.1}C_{0.2})$, which is in accordance with the order in diblock copolymers of $A_{0.5}B_{0.5} < A_{0.6}B_{0.4} < A_{0.7}B_{0.3}$. We attribute this to the specific mechanism of phase separation dynamics in linear triblock copolymers; the middle block (B) with the minority block (A or C) will be first separated from the majority block (C or A), and then block B and block A or C are separated from each other. Therefore, this can be understood very simply by considering that the ODT of linear $A_{0.3}B_{0.3}C_{0.4}$ behaves as that of diblock $A_{0.6}B_{0.4}$, while for star triblock copolymers, the order is

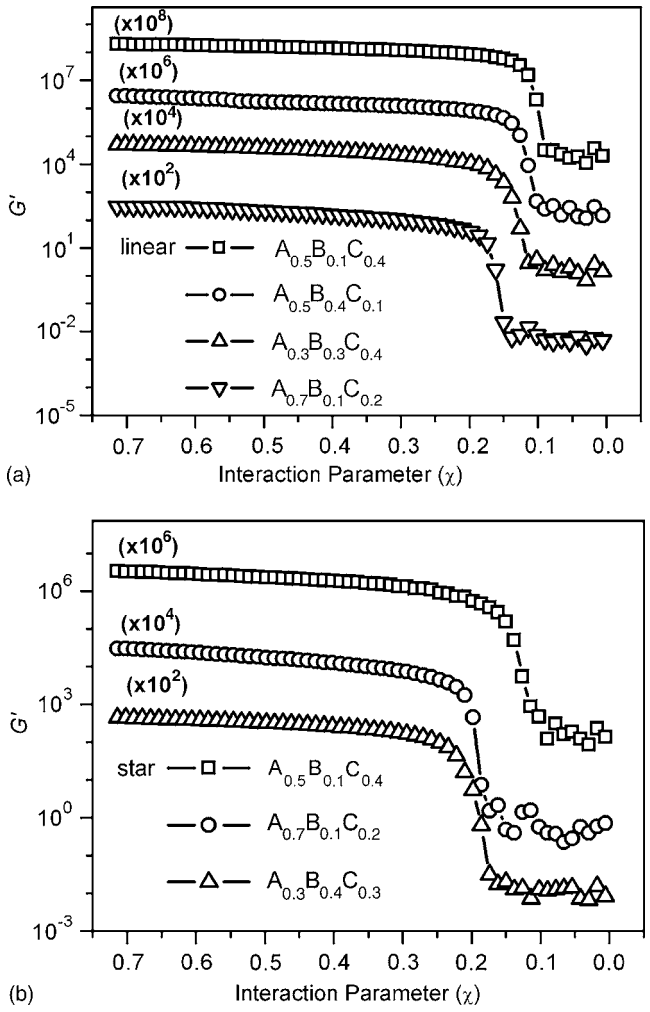

FIG. 7. Simulated temperature sweep of G' (in units of nK_BT/V) for linear ABC (a) and star ABC (b) triblock copolymers in oscillatory shear flow at strain amplitude $\Gamma=0.01$ and reduced frequency of $\omega=0.02$. Data in (a) $A_{0.7}B_{0.1}C_{0.2}$, $A_{0.3}B_{0.3}C_{0.4}$, $A_{0.5}B_{0.4}C_{0.1}$, and $A_{0.5}B_{0.1}C_{0.4}$ are vertically shifted by 2, 4, 6, and 8 decades, respectively, for clarity; data in (b) $A_{0.3}B_{0.4}C_{0.3}$, $A_{0.7}B_{0.1}C_{0.2}$, and $A_{0.5}B_{0.1}C_{0.4}$ are vertically shifted by 2, 4, and 6 decades, respectively.

$\chi_{\mathrm{ODT}}(A_{0.5}B_{0.1}C_{0.4}) < \chi_{\mathrm{ODT}}(A_{0.7}B_{0.1}C_{0.2}) < \chi_{\mathrm{ODT}}(A_{0.3}B_{0.4}C_{0.3})$. In contrast to linear triblock copolymers, the ODT of star terpolymers is generally higher than that of linear ones with the same composition because the constraint of joint core in star triblock copolymers is so strong compared to that in linear triblock ones that star triblocks are not liable to phase separate. Actually, this feature is also reflected in the previous discussion in Fig. 1, in which the response of linear triblock copolymers on shear is stronger than that of the star triblock ones.

As a result, in this scheme, the simulated mechanical properties are able to monitor the scarcely perceivable morphological transforms which introduce distinguishable changes in G'. In particular, as the block copolymer approaches the ODT, the thermodynamic differences of different chain architectures (such as symmetric AB diblock versus ABA triblock copolymers by coupling AB diblocks) are almost indistinguishable in the strong-segregation regime, however, become significantly evident. This is also experimentally investigated by Gehlsen *et al.*[30] Additionally, we should note that this method is capable of predicting the OOT, although it is not found in Fig. 7 due to 2D simulation where more morphological transitions in 3D cannot be obtained.

IV. CONCLUSIONS

To conclude, we introduce the variable cell shape method into DSCFT, which may be used as a tool to investigate the dynamic and mechanical properties of a complex inhomogeneous polymer system. The method adopted in this article is capable of accounting for the inhomogeneity induced changes in the chain conformations and their coupling to the external field such as shear through the chain propagator $q(\mathbf{r},s)$. In other words, the nature of polymer chain is explicitly taken into account in influencing the thermodynamical and rheological properties of complex polymeric system. According to the $q(\mathbf{r},s)$, the distribution of local stress tensor components can be obtained and thus the mechanical properties and rheology correlated with any given complex phases may be calculated.

In this paper, the morphology evolution kinetics in the presence of shear according to the chain conformation is investigated. In agreement with experiments, the chain topology such as linear and star triblock copolymers has a large influence on the structure and dynamics under external shear. Linear triblock copolymers are more flexible to be oriented and extended along the shear direction under shear, while the morphology of star triblock copolymers exhibits less sensitive change upon shear due to the joint core constraint. Preferential lamellar orientation for the linear triblock copolymer is observed under LAOS; increasing shear frequency always prefers perpendicular lamellae, while increasing shear amplitude would prefer the lamellae parallel alignment along the shear direction. Furthermore, since the stress tensor is included in this scheme, by coupling the stress formula in the oscillatory shear measurements, phase separation evolution and corresponding rheological properties are obtained. It is interesting to note that for linear triblock copolymers, the minority middle block B is often trapped in between the interface of two other end blocks to phase separate, leading to the modulus decrease of the middle block in the early stage of phase separation. Similar trap mode can be observed for star terpolymers with one minority block and two majority blocks. Moreover, the storage and loss moduli G' and G'' can be simultaneously determined in frequency sweeps when we do not switched off the diffusion in the simulation process of rheological response. For ordered structure, the low shear stress induced is mostly of elastic origin and the changes of G' are more obvious than those of G''. Finally, our method is further applied to the study of ODT. The simulations show that the χ_{ODT} of linear triblock copolymers is smaller than that of star triblock ones. Extension of this method to 3D with hydrodynamic effects and to inhomogeneous polymer nanoparticle composites and copolymers in confinement is underway in the future work.

ACKNOWLEDGMENTS

We thank financial support from the National Basic Research Program of China (Grant No. 2005CB623800) and the Excellent Research Group of NSF of China (No. 20221402). The NSF of China (Grant Nos. 20474012, 20674012, 20474011 and 20574015) is also acknowledged.

[1] F. S. Bates, MRS Bull. **30**, 525 (2005).
[2] P. Tang, F. Qiu, H. D. Zhang, and Y. L. Yang, Phys. Rev. E **69**, 031803 (2004).
[3] P. Tang, F. Qiu, H. D. Zhang, and Y. L. Yang, J. Phys. Chem. B **108**, 8434 (2004).
[4] Y. Bohbot-Raviv and Z. G. Wang, Phys. Rev. Lett. **85**, 3428 (2000).
[5] F. Drolet and G. H. Fredrickson, Phys. Rev. Lett. **83**, 4317 (1999).
[6] X. A. Li, P. Tang, F. Qiu, H. D. Zhang, and Y. L. Yang, J. Phys. Chem. B **110**, 2024 (2006); R. Wang, P. Tang, F. Qiu, and Y. L. Yang, *ibid.* **109**, 17120 (2005); X. H. He, H. J. Liang, L. Huang, and C. Y. Pan, *ibid.* **108**, 1931 (2004).
[7] F. S. Bates and G. H. Fredrickson, Macromolecules **27**, 1065 (1994); G. H. Fredrickson and F. S. Bates, Annu. Rev. Mater. Sci. **26**, 501 (1996); I. W. Hamley, *The Physics of Block Copolymers* (Oxford University Press, New York, 1998); G. H. Fredrickson, V. Ganesan, and F. Drolet, Macromolecules **35**, 16 (2002).
[8] M. W. Matsen and M. Schick, Phys. Rev. Lett. **72**, 2660 (1994).
[9] Y. Matsumiya, M. Matsumoto, H. Watanabe, T. Kanaya, and Y. Takahashi, Macromolecules **40**, 3724 (2007).
[10] M. Doi and S. F. Edwards, *The Theory of Polymer Dynamics* (Oxford University Press, New York, 1986).
[11] H. Tanaka and T. Araki, Chem. Eng. Sci. **61**, 2108 (2006).
[12] V. Ganesan and V. Pryamitsyn, J. Chem. Phys. **118**, 4345 (2003).
[13] B. Narayanan, V. Pryamitsyn, and V. Ganesan, Macromolecules **37**, 10180 (2004).
[14] J. G. E. M. Fraaije, J. Chem. Phys. **99**, 9202 (1993).
[15] N. M. Maurits, A. V. Zvelindovsky, and J. G. E. M. Fraaije, J. Chem. Phys. **108**, 2638 (1998).
[16] M. B. Kossuth, D. C. Morse, and F. S. Bates, J. Rheol. **43**, 167 (1999); R. B. Thompson, K. O. Rasmussen, and T. Lookman, J. Chem. Phys. **120**, 3990 (2004); C. A. Tyler and D. C. Morse, Macromolecules **36**, 8184 (2003); R. Huang, Y. Jiang, and H. J. Liang, ChemPhysChem **7**, 1950 (2006).
[17] G. H. Fredrickson, J. Chem. Phys. **117**, 6810 (2002).
[18] J. L. Barrat, G. H. Fredrickson, and S. W. Sides, J. Phys. Chem. B **109**, 6694 (2005).
[19] D. M. Hall, T. Lookman, G. H. Fredrickson, and S. Banerjee, Phys. Rev. Lett. **97**, 114501 (2006); J. Comput. Phys. **224**, 681 (2007).
[20] Z. L. Zhang, H. D. Zhang, Y. L. Yang, I. Vinckier, and H. M. Laun, Macromolecules **34**, 1416 (2001).
[21] J. F. Xia, M. Z. Sun, F. Qiu, H. D. Zhang, and Y. L. Yang, Macromolecules **38**, 9324 (2005).
[22] A. V. Zvelindovsky, G. J. A. Sevink, B. A. C. van Vlimmeren, N. M. Maurits, and J. G. E. M. Fraaije, Phys. Rev. E **57**, R4879 (1998).
[23] G. H. Fredrickson and F. S. Bates, Annu. Rev. Mater. Sci. **26**, 501 (1996).
[24] G. Tzeremes, K. O. Rasmussen, T. Lookman, and A. Saxena, Phys. Rev. E **65**, 041806 (2002).
[25] A. Onuki, J. Phys. Soc. Jpn. **66**, 1836 (1997).
[26] M. E. Vigild, C. Chu, M. Sugiyama, K. A. Chaffin, and F. S. Bates, Macromolecules **34**, 951 (2001).
[27] P. Maniadis, T. Lookman, E. M. Kober, and K. O. Rasmussen, Phys. Rev. Lett. **99**, 048302 (2007).
[28] L. Leibler, Macromolecules **13**, 1602 (1980).
[29] A. M. Mayes and M. O. Delacruz, J. Chem. Phys. **91**, 7228 (1989); M. W. Matsen and R. B. Thompson, *ibid.* **111**, 7139 (1999).
[30] M. D. Gehlsen, K. Almdal, and F. S. Bates, Macromolecules **25**, 939 (1992).